UV Resonance Raman Studies of DNA–Pyrene Interactions: Optical Decoupling Raman Spectroscopy Selectively Examines External Site Bound Pyrene

Namjun Cho and Sanford A. Asher*

Contribution from the Department of Chemistry, University of Pittsburgh, Pittsburgh, Pennsylvania 15260

Received November 9, 1992

Abstract: Intercalation of pyrene into DNA results in a strong hypochromism of those pyrene electronic absorption bands which overlap the nucleic acid electronic transitions. The resonance Raman cross sections of pyrene excited within these absorption bands are decreased by factors of 10–100-fold. Raman saturation measurements indicate a dramatic increase in the intercalated pyrene nonradiative relaxation rate, which is consistent with fluorescence quenching observations. We demonstrate using the new technique of optical decoupling Raman spectroscopy (ODRS) that the remaining fluorescence derives from pyrenes not intercalated between bases, but most likely bound externally. ODRS involves a double pulse sequence, where the pump laser excites the sample in a spectral region which is selectively absorbed by one component; the pump selectively excites this component out of its electronic ground state. A probe pulse monitors the Raman spectra of the remaining ground-state species in the sample, in this case selectively enriched in intercalated pyrene. The Raman intensities and enhancement patterns of the intercalated pyrene are very different from the external site bound pyrene. This new technique of ODRS permits us to selectively monitor pyrene molecules bound at two different sites of DNA and is a new general method for studying complex systems.

Introduction

A molecular-level understanding of interactions between polycyclic aromatic hydrocarbons (PAH) and DNA is crucial in order to understand the initial events in the mechanism of PAH-induced chemical carcinogenesis.[1-3] Chemical carcinogenesis induced by PAH involves the covalent attachment of the PAH to DNA. This is thought to be initiated by the intercalation of PAH between nucleic acid bases[4-7] or by binding of PAH to exterior portions of the DNA, such as at the minor groove.[8-10] The chemistry of this initial binding defines the structure of the final covalently bound species, its carcinogenic activity,[11-13] and how it modifies the DNA structure.[14-17]

Numerous techniques have been used to study PAH–DNA binding, such as absorption and fluorescence spectroscopy, CD, and NMR.[3,5-12] The utility of absorption, CD, and emission spectroscopy is limited by the weak spectral signatures associated with binding of PAH to the exterior of DNA, and the difficulty of resolving the spectral information from the low concentrations of the exterior bound PAH, from the majority species intercalated within the DNA.[5,8-11]

In the study here we describe a new technique we call optical decoupling Raman spectroscopy (ODRS) which allows us to selectively examine the vibrational spectrum of either intercalated or exterior bound pyrene; we use pyrene as a model PAH for these studies because it is structurally similar to benzo[*a*]pyrene but is not carcinogenic.[3] We selectively depopulate the ground state of the exterior bound pyrene by using an optical pump pulse, which selectively excites this species; we rely on its long excited-state lifetime to maintain the population in its S_1 excited state, while a probe pulse excites the UV resonance Raman spectra (UVRR) of the intercalated ground-state pyrene. This work follows the recent development of UVRR[18,19] for studying DNA structure[20-25] and for studying PAH.[26-29] The selectivity and sensitivity of these techniques make studies of PAH binding to DNA relatively easy.

Experimental Section

Calf-thymus DNA (Calbiochem. Co.), pyrene (Chem. Service Inc.), sodium dodecyl sulfate (Sigma Chem. Co.), and sodium selenate (Aldrich Chem. Co.) were used without further purification. The samples of DNA

* Author to whom correspondence should be addressed.

(1) Huberman, E.; Sashs, L.; Yang, S. K.; Gelboin, H. V. *Proc. Natl. Acad. Sci. U.S.A.* **1976**, *73*, 607.
(2) Yang, S. K.; McCourt, D. W.; Roller, R. P.; Gelboin, H. V. *Proc. Natl. Acad. Sci. U.S.A.* **1976**, *73*, 2594.
(3) *Polycyclic Hydrocarbons and Carcinogenesis*; Harvey, R. G., Ed.; American Chemical Society: Washington, DC.
(4) Geacintov, N. E. *Carcinogenesis* **1986**, *7*, 759.
(5) Wolfe, A.; Shimer, G. H., Jr.; Meehan, T. *Biochemistry* **1987**, *26*, 6392.
(6) Meehan, T.; Bond, D. M. *Proc. Natl. Acad. Sci. U.S.A.* **1984**, *81*, 2635.
(7) Lin, J.; LeBreton, P. R.; Shipman, L. L. *J. Phys. Chem.* **1980**, *84*, 642.
(8) Chen, F.-M. *Nucleic Acids Res.* **1983**, *11*, 7231; *Carcinogenesis* **1984**, *5*, 753.
(9) Ibanez, V.; Geacintov, N. E.; Gagliano, A. G.; Brandimarte, S.; Harvey, R. G. *J. Am. Chem. Soc.* **1980**, *102*, 5661.
(10) Undeman, O.; Lycksell, P. O.; Graslund, A.; Astlind, T.; Ehrenberg, A.; Jernstrom, B.; Tjerneld, F.; Norden, B. *Cancer Res.* **1983**, *43*, 1851.
(11) Geacintov, N. E.; Zinger, D.; Ivanez, V.; Santella, R.; Grunberger, D.; Harvey, R. G. *Carcinogenesis* **1987**, *8*, 925.
(12) Zinger, D.; Geacintov, N. E.; Harvey, R. G. *Biophys. Chem.* **1987**, *27*, 131.
(13) Harvey, R. G.; Geacintov, N. E. *Acc. Chem. Res.* **1988**, *21*, 66.
(14) Berman, H. M.; Yang, P. R. *Annu. Rev. Biophys. Bioeng.* **1981**, *10*, 87.
(15) Hogan, M. E.; Dattagupta, N.; Whitlock, J. P., Jr. *J. Biol. Chem.* **1981**, *256*, 4504.
(16) Gamper, H. B.; Straub, K.; Calvin, M.; Bartholomew, J. C. *Proc. Natl. Acad. Sci. U.S.A.* **1980**, *77*, 2000.
(17) Drinkwater, N. R.; Miller, J. A.; Miller, E. C.; Yang, N.-C. *Cancer Res.* **1978**, *38*, 247.
(18) Asher, S. A.; Johnson, C. R.; Murtaugh, J. *Rev. Sci. Instrum.* **1983**, *54*, 1657.
(19) (a) Asher, S. A. *Annu. Rev. Phys. Chem.* **1988**, *39*, 537. (b) Asher, S. A. *Anal. Chem.* **1993**, *65*, 59A and 201A.
(20) Fodor, S. P. A.; Spiro, T. G. *J. Am. Chem. Soc.* **1986**, *108*, 3198.
(21) Efremov, R. G.; Feofanov, A. V.; Dzhandzhugazyan, K. N.; Modyanov; N. N.; Nabiev, I. R. *FEBS Lett.* **1990**, *260*, 257.
(22) Perno, J. R.; Grygon, C. A.; Spiro, T. G. *J. Phys. Chem.* **1989**, *93*, 5672.
(23) Kubasek, W. L.; Hudson, B.; Peticolas, W. *Proc. Natl. Acad. Sci. U.S.A.* **1985**, *82*, 2369.
(24) Miskovsky, M.; Chinsky, L.; Laigle, A.; Turpin, P. Y. *J. Biomol. Struct. Dyn.* **1989**, *6*, 915.
(25) Grygon, C. A.; Spiro, T. G. *Biochemistry* **1989**, *28*, 4397.
(26) Asher, S. A. *Anal. Chem.* **1984**, *56*, 720.
(27) Asher, S. A.; Johnson, C. R. *Science* **1984**, *225*, 311.
(28) Johnson, C. R.; Asher, S. A. *Anal. Chem.* **1984**, *56*, 2258.
(29) Jones, C. M.; Asher, S. A. *J. Chem. Phys.* **1988**, *89*, 2649.

0002-7863/93/1515-6349$04.00/0

containing intercalated pyrene were prepared by adding solid pyrene to DNA aqueous solutions and then stirring for 2 days at 4 °C. The mixture was centrifuged twice at 25 000 rpm for 40 min to remove excess solid pyrene.[8] Pyrene was dissociated from DNA by addition of 1% sodium dodecyl sulfate (SDS), which extracted the intercalated pyrene into SDS micelles. The amount of pyrene bound to the DNA was determined from absorption measurements of the DNA–pyrene solution after addition of 1% SDS; we utilized our measured molar absorptivity of 45 540 M^{-1} cm^{-1} at 336.4 nm for pyrene in SDS micelles. The DNA base concentration was determined from absorption measurements by using a nucleic acid absorptivity[5] at 260 nm of 6550 M^{-1} cm^{-1}. The DNA and pyrene concentrations were 2.14 mM and 28.7 μM, respectively, giving a DNA base to pyrene ratio of *ca.* 75:1.

Absorption spectra were obtained by using a Perkin-Elmer Lambda 9 UV–visible–near-IR spectrophotometer. We measured the samples in 0.5-mm cells. Fluorescence emission and excitation spectra were obtained using an SLM/Aminco 8000 C spectrofluorometer. The UV Raman instrumentation used is described in detail elsewhere.[18,30] For the 240-nm Raman measurements, a Lambda Physik model EMG 103 XeCl excimer laser was used to produce 308-nm, 100-Hz pulses with a *ca.* 16-ns pulse width, which pumped a Lambda Physik FL 3002 dye laser. The dye laser output was frequency doubled with a β-barium borate doubling crystal to yield 240 nm. For 272-nm excitation a frequency-doubled Quanta-Ray DCR-2A Nd:YAG laser was used to generate *ca.* 4-ns, 20-Hz pulses, which pumped a Quanta-Ray Model PDL-1 dye laser. The dye laser output was frequency doubled with a KDP doubling crystal to yield 272 nm. For the pump–probe experiments the Nd:YAG laser system 310-nm frequency-doubled dye output was used as a pump beam, while the 240-nm probe beam was obtained by mixing the 310-nm output with the 1064-nm YAG fundamental. The doubled and mixed beams were separated by a Pellin-Broca dispersion prism and independently aligned to temporally and spatially overlap on the sample and to maximize the Raman signal. The 244-nm CW excitation was obtained from an intracavity frequency-doubled Coherent Inc. Ar^+ laser, which has been described in detail recently.[30]

The *ca.* 35-mL sample solutions used for the Raman measurements were pumped through a 1.0-mm-i.d. Suprasil quartz capillary by using a syringe pump in order to provide fresh sample to the illuminated sample volume between laser pulses. The excitation beam was focused by a 25-cm focal-length lens; the beam diameter was *ca.* 1 mm at the sample surface. The scattered light was collected in a 135° back-scattering geometry and focused onto the entrance slit of a Spex Triplemate spectrometer using an ellipsoidal mirror. A crystalline quartz wedge was used to avoid any monochromator polarization bias by randomizing the polarization of light entering the spectrometer. The laser average power and the pulse energy were measured by using a Scientech Model 361 power meter. Suprasil neutral density filters (Melles Griot) were used to attenuate the laser pulse energy flux to 1-30 mJ/cm^2 at the sample surface. We measured the absorption spectra of the solutions before and after laser illumination to check for any irreversible damage. No significant spectral changes were observed.

The Raman intensities of the pyrene bands were measured relative to the 1486-cm^{-1} DNA band, and the differential Raman cross sections were calculated by extrapolating the relative intensity ratios to zero excitation energy flux.[31-33] The Raman intensity of the 1486-cm^{-1} DNA band increased linearly with increasing incident energy flux under our experimental conditions. The Raman cross section of the DNA band was determined by using selenate, SeO_4^{2-}, as the internal intensity standard.[34] The relative intensity ratios of the analyte bands to the internal intensity standard band used for our calculations derived from peak height measurements.[35] The calculated Raman cross sections were corrected for the throughput efficiencies of the spectrometer and detector sensitivity. We utilized the Raman saturation methodology described by Teraoka et al.[31,33] and the BMDP 3R nonlinear least squares regression programs for determining the ground-state repopulation rates and Raman cross sections.

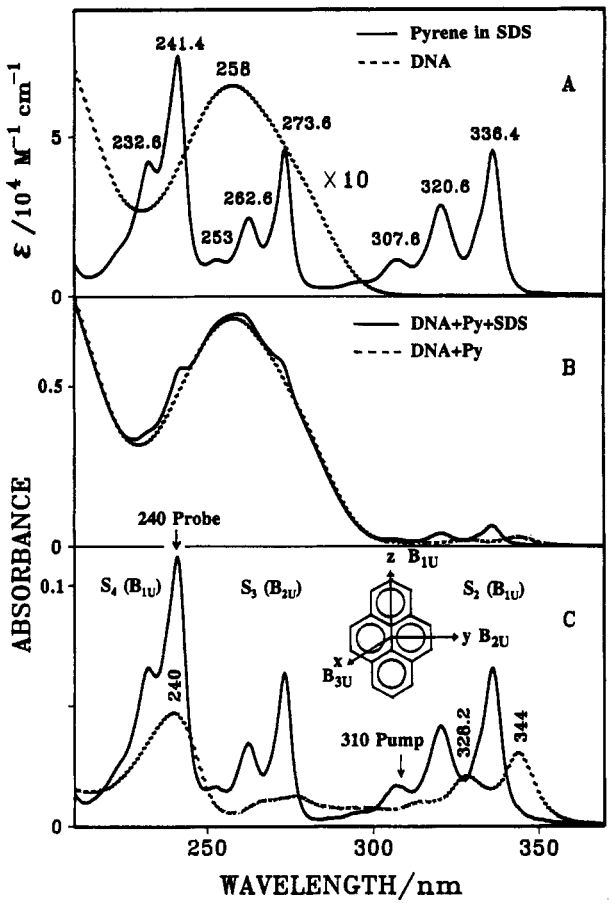

Figure 1. (A) Comparison of UV absorption spectra of an aqueous solution of calf-thymus DNA (dotted line) and an aqueous solution of pyrene in 1% SDS (solid line). The DNA spectrum shown has been scaled up 10-fold. (B) Absorption spectra of an aqueous solution of pyrene in calf-thymus DNA (dotted line) and the same solution after addition of 1% SDS (solid line). A 0.5-mm pathlength UV cell was used. The nucleic acid base and pyrene concentrations are 2.14×10^{-3} and 2.87×10^{-5} M, respectively. (C) Absorption difference spectra were obtained by subtracting the DNA absorption spectrum from that of pyrene in DNA (dotted line) and from the spectrum of pyrene in DNA with 1% SDS (solid line). Also shown are the pump and probe excitation wavelengths for the Raman decoupling studies.

Results

Figure 1A shows the electronic absorption spectra of aqueous solutions of calf-thymus DNA and of pyrene in SDS micelles. The absorption spectrum of calf-thymus DNA shows a broad absorption band with a maximum at 258 nm, which results from the π–π^* electronic transitions of the purine and pyrimidine rings of adenine (A) and guanine (G), thymine (T) and cytosine (C). Calf-thymus DNA contains 56% A-T base pairs and 44% G-C base pairs.[20] The electronic transitions of DNA bases have been described elsewhere.[36] Pyrene has a rich absorption spectrum showing strong Franck–Condon vibronic progressions.[26,29] The strong dipole-allowed π–π^* electronic transitions to the S_2, S_3, and S_4 excited states of pyrene in SDS occur at 336.4 nm (B_{1U}), 273.6 nm (B_{2U}), and 241.4 nm (B_{1U}), respectively. The weak S_1 (B_{1U}) pyrene electronic transition occurs at 372 nm; the transition is symmetry-allowed but is orbitally forbidden. Its absorptivity derives mainly from vibronic coupling. The pyrene S_3 and S_4 electronic transitions overlap the DNA absorption band.

Figure 1B shows the electronic absorption spectra of a sample of pyrene in DNA (dotted line) and the same sample after 1% SDS was added (solid line). Compared to pyrene in the SDS micelles, the pyrene in DNA shows an 8-nm red-shift and a *ca.*

(30) Asher, S. A.; Bormett, R. W.; Chen, X. G.; Lemmon, D. H.; Cho, N.; Peterson, P.; Arrigoni, M.; Spinelli, L.; Cannon, J. *Appl. Spectrosc.* **1993**, *47*, 628.
(31) Teraoka, J.; Harmon, P. A.; Asher, S. A. *J. Am. Chem. Soc.* **1990**, *112*, 2892.
(32) Johnson, C. R.; Ludwig, M.; Asher, S. A. *J. Am. Chem. Soc.* **1986**, *108*, 905.
(33) Harmon, P. A.; Teraoka, J.; Asher, S. A. *J. Am. Chem. Soc.* **1990**, *112*, 8789.
(34) Song, S.; Asher, S. A. *Biochemistry* **1992**, *30*, 1199.
(35) Dudik, J.; Johnson, C. R.; Asher, S. A. *J. Chem. Phys.* **1985**, *82*, 1732.
(36) Callis, P. R. *Annu. Rev. Phys. Chem.* **1983**, *34*, 329. Lipinski, J. *Spectrochim. Acta* **1989**, *45A* (5), 557.

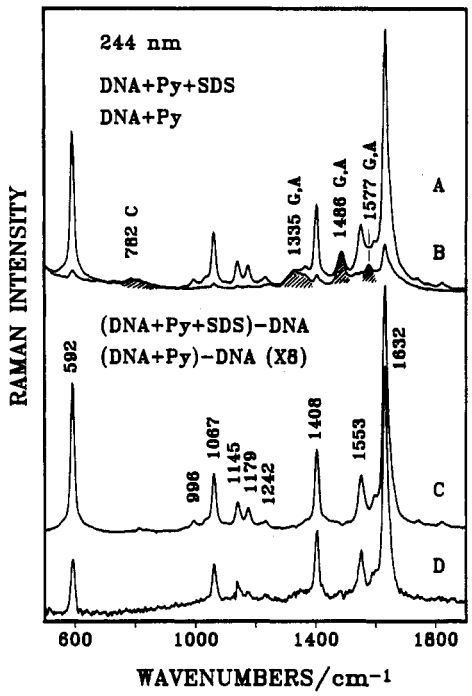

Figure 2. The 244-nm excited resonance Raman spectra of (A) a sample of pyrene and DNA containing 1% SDS and (B) a sample of pyrene in DNA. Difference spectra showing contribution of pyrene in (C) SDS micelles and (D) DNA obtained by subtracting the spectrum of calf-thymus DNA. The concentrations of DNA and pyrene are 2.3×10^{-3} and 3.3×10^{-5} M, respectively. The spectra are normalized to the intensity of the 1486-cm^{-1} DNA band for comparison. The DNA bands are shaded. The laser excitation utilized a new CW laser. The incident laser power was 40 mW, which corresponded to a power density of 15 W/cm^2. Spectral resolution: 11.4 cm^{-1}. Accumulation time: 10 min.

50% S_2 absorption decrease; this has been used as a signature of pyrene intercalation between DNA bases.[8-10] After addition of SDS, the pyrene S_3 and S_4 absorption maxima become evident as shoulders overlapping the broad DNA absorption band. Figure 1C shows the absorption difference spectra obtained by subtracting off the absorption spectrum of an aqueous calf-thymus DNA solution. The S_3 transition disappears almost completely, and the S_4 transition exhibits a loss of vibronic fine structures and weakens by 60%.

Figure 2 shows the 244-nm excited resonance Raman spectra of a sample of pyrene bound to DNA (B) and this same sample after addition of 1% SDS (A). Figure 2C,D shows difference spectra where the contribution of DNA is numerically removed. The strongest pyrene Raman bands appear at 592, 1067, 1179, 1408, 1553, and 1632 cm^{-1}. Table I lists the observed bands, the previous assignments by Mecke and Klee, and the symmetry assignments which derived from depolarization ratio measurements by Bree et al.[29,37,38] The spectrum observed for pyrene in SDS micelles is similar to that of pyrene in organic solvents.[29] The Raman cross sections of all of the pyrene bands dramatically decrease upon intercalation into DNA. The 240-nm Raman cross section of the pyrene 1632-cm^{-1} band in DNA is only 0.17-fold as large as that in the SDS micelles; this ratio is almost the same as the ratio (0.18) of the squares of the molar absorptivities at 240 nm. The Raman hypochromism ratio is expected to scale as the square of the absorption hypochromism ratio for an *A*-term resonance Raman enhancement mechanism.[39] In contrast, the Raman hypochromism ratio for the 592-cm^{-1} band is 0.04. The Raman hypochromism ratios are listed in Table II.

The 244-nm excited DNA Raman bands derive from vibrations of the purine and pyrimidine rings. The strongest band at 1486 cm^{-1} derives from the overlapping 1482- and 1489-cm^{-1} bands of adenine and guanine.[20,40] The assignment of each band to the DNA bases is indicated in the figures.

Figure 3 shows the dependence of the Raman intensity of the pyrene 1632- and 592-cm^{-1} bands on the excitation wavelength. Pyrene in SDS micelles shows a behavior similar to that observed by Jones and Asher[29] for pyrene in acetonitrile; the excitation profile maximum occurs close to the pyrene absorption maximum, and the 592-cm^{-1} band has a narrower excitation profile than the 1632-cm^{-1} band, which has significant intensity for shorter wavelength excitations. In contrast, the excitation profiles for the pyrene in DNA are broad and similar for the 1632- and 592-cm^{-1} bands, and no maximum is evident. This alteration in the excitation profile occurs in parallel with the broadened S_4 absorption band of pyrene in DNA observed in Figure 1.

Figure 4 shows the 272-nm excited resonance Raman spectra. The prominent Raman bands of pyrene occur at 592, 1068, 1242, 1408, and 1597 cm^{-1}. The 272-nm excited pyrene Raman band intensities decrease much more dramatically upon binding to DNA than was observed with 240-nm excitation (not shown). The strongest bands at 592 and 1408 cm^{-1} show more than a 25-fold decrease in Raman cross section, while the other bands disappear almost completely. This large Raman hypochromism correlates with the large absorption hypochromism evident in

Table I. Fundamental Frequencies and Vibrational Assignments of Pyrene

freq (cm^{-1})	sym[a]	vib type[b]	freq (cm^{-1})	sym	vib type
221	B_{2g}		1233	A_g	
256	B_{1g}		1242	A_g	
408	A_g	w[d]	1327	A_g	
458	B_{3g}?[c]		1351	A_g	
505	B_{3g}		1358	A_g	
592	A_g	w	1370	B_{3g}	
737	B_{3g}		1395	A_g	
773	B_{2g}		1408	A_g	w
802	A_g		1426	A_g	w
844	B_{2g} or B_{3g}		1462	A_g	
904	?		1504	A_g	
958	B_{2g} or B_{3g}		1553	A_g	
970	B_{2g}?		1562	A_g	
1006	A_g		1597	B_{3g}	w
1040	A_g		1632	A_g	w
1067	A_g	δ[e]?	1647	A_g	
1110	B_{3g}		1665	A_g	
1145	A_g	δ	1697	A_g	
1174	B_{3g}?	w?	3024	A_g	
1192	A_g		3059	A_g	
1199	A_g		3103	A_g	
1212	A_g				

[a] See ref 37. [b] See ref 38. [c] ?: Tentative assignment. [d] w: Vibration involving motion of the carbon atoms in the molecular plane. [e] δ: Vibration involving a change in the angle between two neighboring carbon atoms and a hydrogen bonded to one of the carbons.

Table II. Pyrene Raman Cross Sections and Raman Hypochromism Ratios upon Binding to DNA (for 240-nm Excitation)

	Raman cross section (b/sr)			estimated σ_R of Py	
cm^{-1}	Py in DNA + SDS	Py in DNA	hypochromism ratio[a] $\sigma_{Py\ in\ DNA}/\sigma_{Py\ in\ SDS}$	intercalated	external site bound
592	53.77	2.38	0.04	0.3	31
996	7.05				
1067	18.39	1.26	0.07	0.3	13
1145		0.93			
1179	31.78				
1408	16.29	1.96	0.12	0.7	16
1553	12.80	1.53	0.12	0.5	13
1632	41.63	7.23	0.17	2.8	50

[a] The 240-nm absorption hypochromism ratio of pyrene in DNA relative to that in SDS micelles is estimated to be 0.42.

(37) Bree, A.; Kydd, R. A.; Misra, T. N.; Vilkos, V. V. B. *Spectrochim. Acta* **1971**, *A27*, 2315.
(38) Mecke, R.; Klee, W. E. *Z. Electrochem.* **1961**, *65*, 327.
(39) Small, E. W.; Peticolas, W. L. *Biopolymer* **1971**, *10*, 69.
(40) Fodor, S. P. A.; Rava, R. P.; Hays, T. R.; Spiro, T. G. *J. Am. Chem. Soc.* **1985**, *107*, 1520.

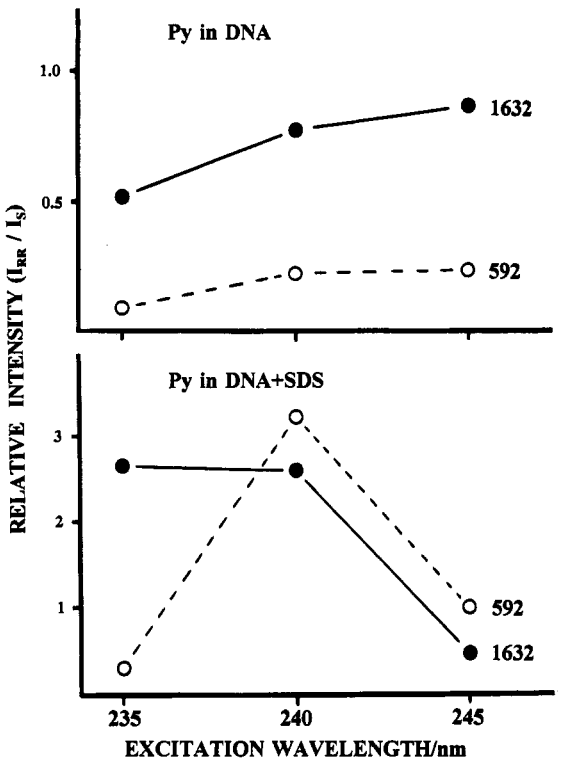

Figure 3. Raman excitation profile of the 592- and 1632-cm^{-1} pyrene bands of pyrene in DNA and in SDS micelles. The ordinate is the ratio of the intensity of pyrene to the internal standard selenate bands.[34] For pyrene in DNA in both the presence and absence of SDS, we used the 1486-cm^{-1} DNA band as the internal intensity standard. In a separate measurement we determined the Raman cross sections of this DNA band relative to the selenate band for a sample containing only DNA and selenate.

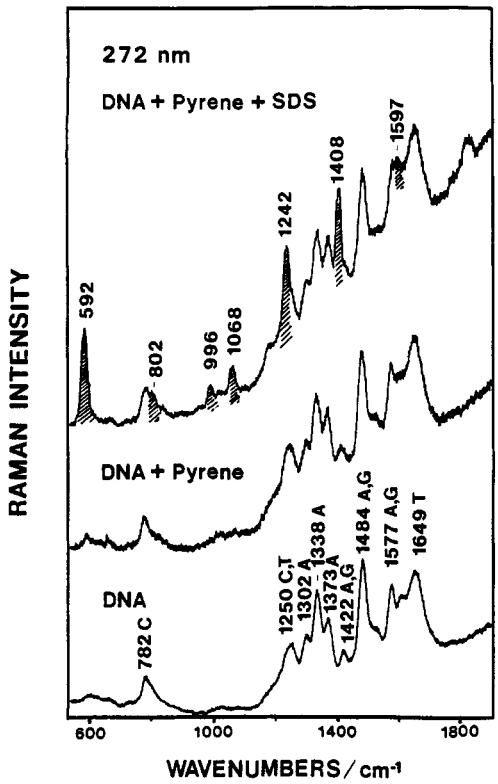

Figure 4. The 272-nm excited resonance Raman spectra of a sample of pyrene and DNA containing 1% SDS, a sample of pyrene in DNA, and a sample containing just calf-thymus DNA. The concentrations of DNA and pyrene are 2.27×10^{-3} and 2.06×10^{-5} M, respectively. The spectra are normalized to the intensity of the 1484-cm^{-1} DNA band for comparison. The pyrene bands are shaded. Pulse energy flux: 5 mJ/cm^2. Spectral resolution: 18 cm^{-1}. Accumulation time: 30 min.

Figure 1. For 272-nm excitation, the most prominent DNA bands at 1338 and 1484 cm^{-1} derive from adenine and overlapping contributions from a 1482-cm^{-1} band of adenine and a 1489-cm^{-1} band of guanine. The 782-cm^{-1} band derives from a cytosine ring breathing mode, which is relatively intense at this excitation wavelength.[20,40]

Figure 5 shows the 240-nm excited resonance Raman spectra of pyrene in SDS (A) and pyrene in DNA (B) as a function of laser pulse energy flux density. Figure 5A shows that the Raman intensities of pyrene in SDS micelles decrease relative to the 835-cm^{-1} internal standard selenate band as the pulse energy flux density increases. This saturation of the pyrene intensities results from depletion of the pyrene ground-state population during the laser pulse excitation[29-31] as excited states are populated.[32,41] The difference spectrum in Figure 5A shows phototransient bands at 580 and 1622 cm^{-1}, which may derive either from the S_1 excited state or from a cation radical. Although the S_1 origin is most likely, quasiline absorption spectra of pyrene[42] show no evidence for a band at 1622 cm^{-1}. These phototransient bands may derive from a pyrene cation radical which can be produced by a sequential two-photon photoionization process which involves S_1 as an intermediate level.[43-45]

Figure 5B shows the dependence of the 240-nm excited pyrene Raman intensities on the pulse energy flux density for pyrene bound to DNA. The pyrene intensities decrease relative to the DNA bands as the energy flux density increases. The difference spectrum shows only bands which result from the decrease in pyrene intensities, without any evidence for phototransient contributions.

We determined the ground-state repopulation rate of pyrene using Raman saturation spectroscopy.[31,33] This technique monitors the ground-state depletion by examining the dependence of the analyte Raman band intensities relative to the internal standard intensities upon the incident energy flux density. Part A and B of Figure 6 show how the relative Raman intensities depend upon the pulse energy flux density for a sample containing pyrene intercalated into DNA and for the same sample after addition of SDS. The intercepts at zero energy flux density are proportional to the ratios of the Raman cross sections of the pyrene bands relative to that of the DNA 1486-cm^{-1} band. We used the DNA 1486-cm^{-1} band as an internal intensity standard, since the DNA Raman bands show no saturation at these pulse energy flux densities. The DNA 1486-cm^{-1} band Raman cross section is 65 mb/sr (mb ≡ millibarns), which was calculated from the intensity ratio of this DNA band to the 835-cm^{-1} internal intensity standard selenate band. The Raman cross sections of the 240-nm excited pyrene bands were calculated from the relative intensity ratios extrapolated to zero energy flux and are listed in Table II. Except for the 592-cm^{-1} band of pyrene intercalated into DNA, all of the other pyrene bands seem to saturate together. The amount of saturation for pyrene in micelles is much greater than for pyrene in DNA. The unique saturation of the 592-cm^{-1} pyrene band suggests that a subpopulation of pyrene with a large 592-cm^{-1} cross section has a uniquely slow relaxation rate (vide infra).

Figure 7 shows the nonlinear least squares fit of the saturation of the pyrene 1408-cm^{-1} band to the Raman saturation model.[31] The open circles (A) are for pyrene intercalated in DNA, while the closed circles (B) are for pyrene in SDS micelles. The relative intensity ratios appear to decrease linearly in the low pulse energy flux range, but then flatten out at pulse energy flux densities above 15 mJ/cm^2. At high energy fluxes, the photon-driven relaxations begin to contribute to the ground-state repopulation rates. The excited-state relaxation rate of pyrene bound to DNA

(41) Jones, C. M.; Devito, V. L.; Harmon, P. A.; Asher, S. A. *Appl. Spectrosc.* **1987**, *41*, 1268.
(42) Klimova, L. A. *Opt. Spectrosc.* **1963**, *15*, 185.
(43) Hall, G. E.; Kenney-Wallace, G. A. *Chem. Phys.* **1978**, *28*, 205.
(44) Richard, J. T.; West, G.; Thomas, J. K. *J. Phys. Chem.* **1970**, *74*, 4137.
(45) Ottolenghi, M. *Chem. Phys. Lett.* **1971**, *10*, 339.

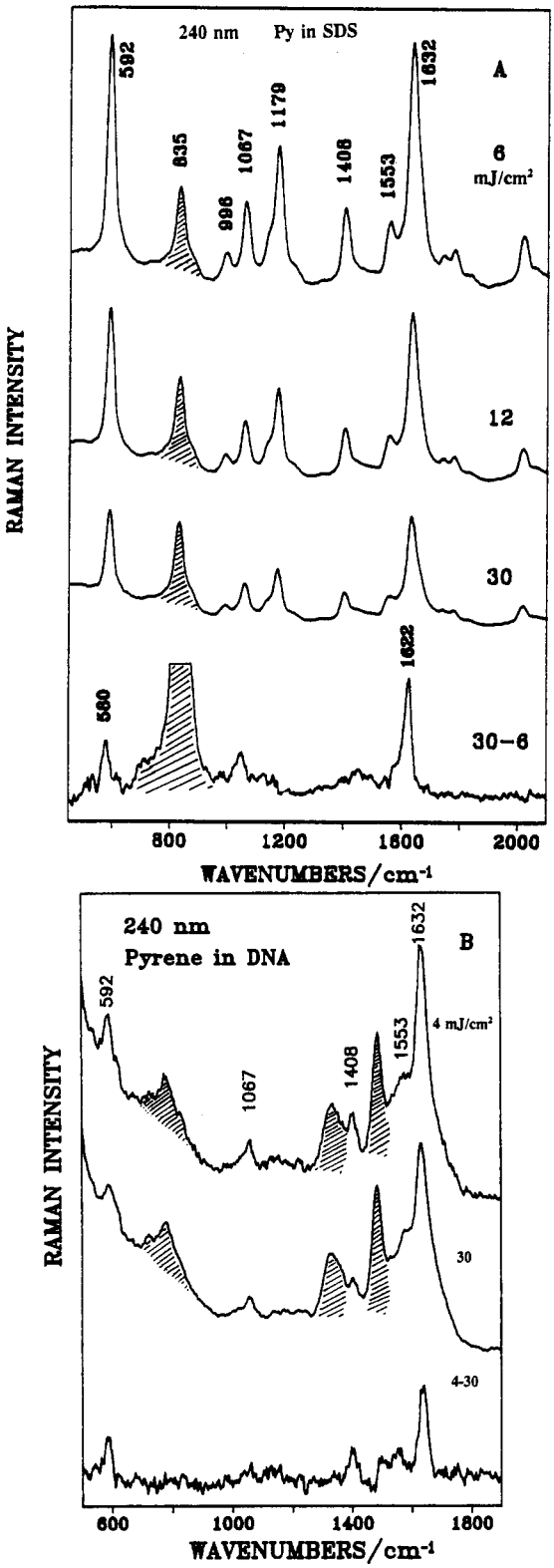

Figure 5. (A) The 240-nm excited resonance Raman spectra of an aqueous solution of 2.6×10^{-5} M pyrene in 1% SDS with 0.1 M sodium selenate. From top to bottom the incident pulse energy flux densities are 6 mJ/cm², 12 mJ/cm², and 30 mJ/cm². The spectra are normalized with respect to the 835-cm^{-1} internal intensity standard selenate band. The difference spectrum shown was obtained by normalizing the high and low pulse energy density spectra to the intensity of the 1632-cm^{-1} band. (B) Energy flux density dependence of the Raman intensities of pyrene in calf-thymus DNA. The concentrations of DNA and pyrene are 2.14×10^{-3} and 2.87×10^{-5} M, respectively. The spectra are normalized to the intensity of the 1486-cm^{-1} DNA band for comparison. The DNA bands are shaded. Pulse energy flux values are 4 and 30 mJ/cm². Spectral resolution; 23.6 cm^{-1}. Accumulation time: 30 min. The difference spectrum was calculated by normalizing to the 1486-cm^{-1} DNA band intensity.

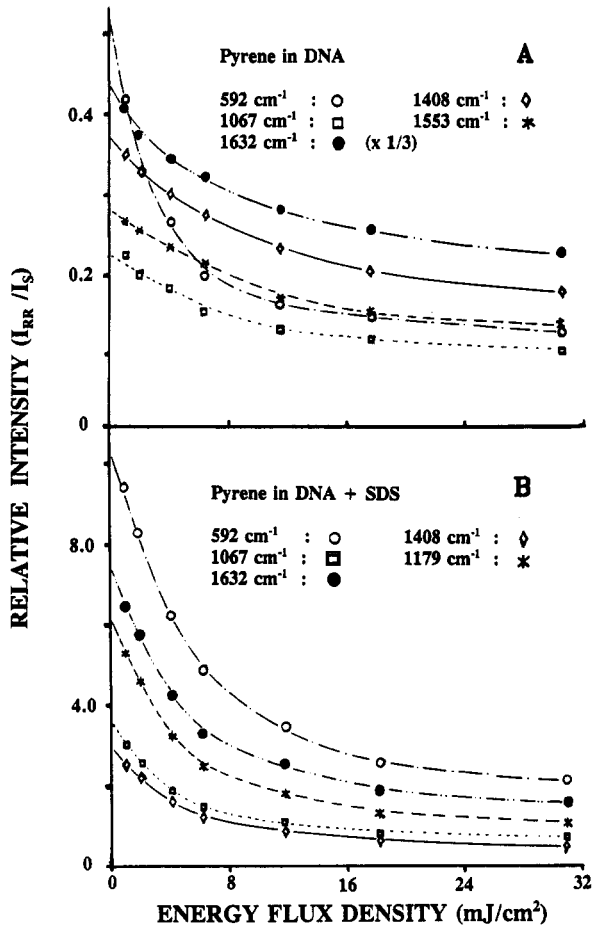

Figure 6. Raman saturation plots at 240-nm excitation showing the dependence of the ratios of the pyrene band intensities relative to the intensity of the DNA 1486-cm^{-1} band for (A) pyrene in DNA and (B) a sample of pyrene, DNA, and 1% SDS. The concentrations of DNA and pyrene are 2.14×10^{-3} and 2.87×10^{-5} M, respectively.

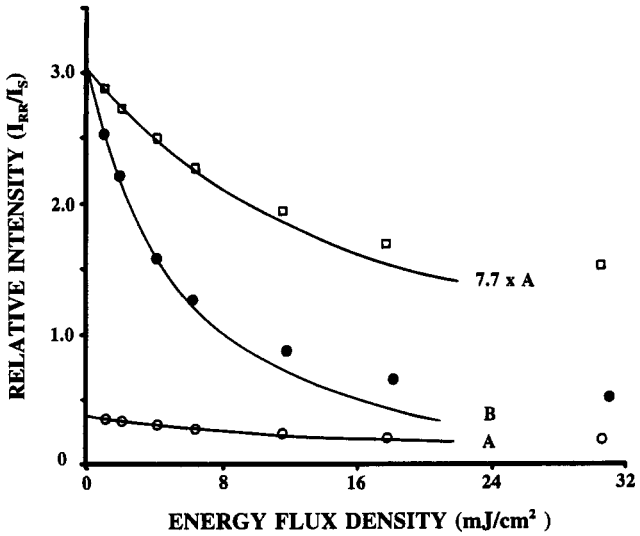

Figure 7. Plot of Raman saturation of the pyrene 1408-cm^{-1} band (240-nm excitation). The solid lines show the nonlinear least squares fit to the Raman saturation model.[31,33] (A) Open circles: pyrene in DNA. (B) Closed circles: pyrene, DNA, and 1% SDS. (C) Curve A has been scaled up by a factor of 7.7 for ease of visual comparison (open squares). These saturation plots utilized the 1486-cm^{-1} DNA band as the internal standard (I_S).

is found to be 1/11 ns for the 1632-, 1408-, and 1067-cm^{-1} bands, which is *ca.* 35-fold higher than for pyrene in SDS micelles. This increased ground-state relaxation rate derives from an increased nonradiative pyrene relaxation rate induced by the DNA bases

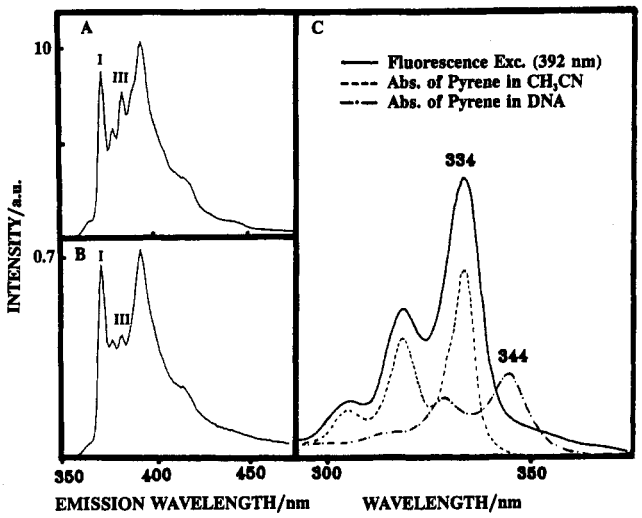

Figure 8. Fluorescence emission spectrum of (A) pyrene in DNA and (B) pyrene, DNA, and 1% SDS. (C) Fluorescence excitation spectrum of pyrene in DNA (solid line) compared to the absorption spectra of pyrene in DNA (dotted line) and pyrene in acetonitrile (dot–dashed line).

Table III. Fluorescence Emission Intensity Ratios for Pyrene in Micelles and Several Solvents

	I/III ratio	
solvent	this work	ref 46
CH_3CN	1.78	1.67
H_2O		1.59
methanol		1.27
ethanol	1.19	
SDS		1.14
CTAB		1.30
dodecane		0.60
DNA	1.63	
SDS + DNA	1.15	

which also results in fluorescence quenching. We were unable to fit the 592-cm^{-1} pyrene band saturation behavior within the reasonable parameters of our model and the average DNA absorption cross sections of Figure 1. However, we can obtain a fit if we increase the absorption cross section of the extensively saturating pyrene species giving rise to the 592-cm^{-1} band.

Figure 8A shows the fluorescence emission spectrum of pyrene within SDS micelles in the presence of DNA, while Figure 8B shows the emission spectrum of pyrene in DNA. The pyrene fluorescence intensity in the absence of SDS is *ca.* 7% of that in the presence of SDS. The fluorescence emission intensity ratio of band I to band III, which is known to strongly depend on the local environment,[46] differs between pyrene in DNA (1.63) and pyrene in SDS (1.15). Table III lists the pyrene I/III band intensity ratios in different solvents. Figure 8C compares the fluorescence excitation spectrum of pyrene in DNA to the absorption spectrum of pyrene in acetonitrile and pyrene intercalated in DNA. The fact that the fluorescence excitation spectrum differs from the intercalated pyrene absorption spectrum indicates that most of the fluorescence from the pyrene bound to the DNA derives from those pyrene species which are not intercalated between DNA bases. These are probably pyrenes bound to an external site.[8-10]

We used pump–probe experiments to selectively examine those pyrene molecules not intercalated between DNA bases. Since the nonintercalated pyrene fluoresces, it must have a longer S_1 lifetime. We selectively saturated out the external site bound pyrene by exciting the sample with a pump beam at 310 nm, where the intercalated pyrene absorbs less than the fluorescent pyrene. The resonance Raman spectrum was excited by a 240-nm probe beam. Figure 9 shows the 240-nm excited Raman spectra in the presence or absence of the 310-nm pump excitation, and the difference spectra between them. At low probe energy flux density (5 mJ/cm^2), the pyrene Raman intensities without the pump excitation are larger than in the presence of the 60 mJ/cm^2 310-nm pump excitation (Figure 9A). The 310-nm pump excitation depletes the ground-state concentration of those pyrene species with the longest excited-state lifetime. The difference spectrum indicates that this pyrene species has a higher relative 592-cm^{-1} band intensity than that of the pyrene intercalated into DNA (see Figure 2). In fact, the difference spectrum is essentially identical to that of the saturating pyrene difference spectrum shown in Figure 5B. At high probe energy flux density (32 mJ/cm^2), the pyrene band intensities are independent of pump excitation (Figure 9B), since the 240-nm probe energy flux density is high enough to saturate the long-lived pyrene species.

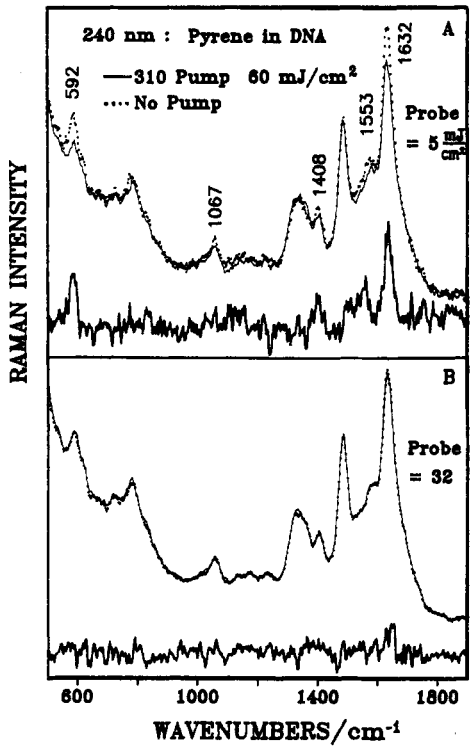

Figure 9. Raman optical decoupling spectra of pyrene in DNA. The 240-nm excited UVRR spectra of pyrene in DNA in the presence (solid line) and absence (dotted line) of a simultaneous 60 mJ/cm^2 pump excitation at 310 nm. Also shown are the difference spectra. Incident probe energy fluxes: (A) 5 mJ/cm^2; (B) 32 mJ/cm^2.

Discussion

Binding Modes and Hypochromism. Pyrene and related polycyclic aromatic hydrocarbons are known to have two modes of binding to DNA.[8-10] Binding mode I, which predominates and involves intercalation, is characterized by a *ca.* 10-nm S_2 absorption spectral red shift and a large absorption hypochromism, in addition to fluorescence quenching and a negative linear dichroism. Type II binding, which involves external binding and probably involves binding to the narrow and deep minor groove in the DNA duplex, results in only small absorption spectral changes, little change in the fluorescence quantum yield or decay time, and an emission which shows oxygen quenching.

The large pyrene absorption hypochromism shown in Figure 1 results from intercalation of the pyrene between the bases; the dramatic 80% S_3 and 60% S_4 absorption band hypochromism results from π-stacking excitonic interactions between the pyrene and DNA bases.[47,48] Pyrene predominantly intercalates between

(46) Kalyanasundaram, K.; Thomas, J. K. *J. Am. Chem. Soc.* **1977**, *99*, 2039.

(47) Tinoco, I., Jr. *J. Am. Chem. Soc.* **1960**, *82*, 4785; *J. Chem. Phys.* **1960**, *33*, 1332.

(48) Rhodes, W. *J. Am. Chem. Soc.* **1961**, *83*, 3609.

DNA base pairs in the duplex region, preferentially at alternating dA-dT base sequences.[8-10]

With 240-nm excitation in the pyrene S_4 electronic transition, we observe a Raman hypochromism for the 1632-cm^{-1} band of 0.17 for pyrene in DNA compared to pyrene in SDS micelles; this is almost the same as the square of the absorption hypochromism (0.42). In contrast, the 592-cm^{-1} band shows a Raman hypochromism of 0.04. If no shift of the resonance absorption occurs, a similar hypochromism should occur for each band. Typically, the Raman hypochromism scales as the square of the absorption hypochromism for symmetric vibrations, which are generally enhanced via an *A*-term mechanism. The increased 592-cm^{-1} band hypochromism results because it has a much narrower excitation profile than does the 1632-cm^{-1} band.[29] The widening of the absorption broadens the excitation profile of all the Raman bands; however, the largest intensity decrease will occur for those bands with the initially narrowest excitation profile width.

Raman Saturation

The Raman saturation results indicate that the ground-state depletion of pyrene complexed to DNA is much less than that of pyrene in SDS micelles. We can quantitatively compare the ground-state relaxation rates by using the Raman saturation methodology[31,33] in which we monitor the photophysical relaxation rate to the ground state by monitoring the Raman intensity dependence upon the incident laser pulse energy flux density. The relative Raman intensity ratio of the pyrene band to the internal standard band depends upon the relative ground-state populations during the incident laser pulse duration. The extent of pyrene ground-state depopulation depends upon its absorption cross section, its relaxation rate back to the ground state, the laser pulse duration, and the incident energy flux density. The ground-state repopulation rate, K, of pyrene is obtained from fitting the relative intensity ratios, I_{RR}/I_S, versus the pulse energy flux density, I_0, data to the saturation model. Also, the pyrene band Raman cross sections can be calculated from the intercept value. As seen in Figure 7, the I_{RR}/I_S versus I_0 data fits the saturation model at low-energy flux, but deviates from this saturation model at high-energy flux, due to photon-driven relaxations.[31] Thus, we only use the low pulse energy flux data in order to calculate the ground-state repopulation rate.

We obtain a ground-state repopulation rate of pyrene in DNA of 1/11 ns for the 1632-, 1408-, and 1067-cm^{-1} bands, which is much faster than the 1/360 ns fluorescence lifetime of pyrene in SDS micelles.[49] This dramatic increase in the pyrene ground-state repopulation rate upon binding to DNA derives from the increased nonradiative relaxation rate induced by ground-state complex formation with DNA bases, which also results in fluorescence quenching. The mechanism of the fluorescence quenching upon intercalation of pyrene into DNA is not understood; Isenberg et al. suggest that it might be due to transient excited-state electron transfer to DNA.[50,51]

Our calculated ground-state repopulation rate of pyrene in DNA is an average value over all pyrenes in the sample (28.7 μM) which includes site I-bound (intercalated), site II-bound (external site bound), and pyrene dissolved in water (soluble to a concentration of 0.3 μM[5]). According to LeBreton, the binding constant of pyrene to site I is about 9 times higher than that to site II.[52] This is reasonably consistent with our fluorescence measurement, which shows that *ca.* 7% of the pyrene fluorescence remains unquenched and that the fluorescence excitation spectrum does not resemble the absorption spectrum of intercalated pyrene, but is similar to the spectrum of pyrene in organic solvents, which should be similar to the expected absorption spectrum of extenal site bound pyrene. The fluorescent pyrene shows little hypochromism in its S_3 absorption since it does not stack with the nucleic acid bases. The intercalated pyrene which is in a hydrophobic environment shows little fluorescence. These results indicate that *ca.* 93% of pyrene intercalates between DNA base pairs while *ca.* 7% binds to a different site, presumably the minor groove.

The 592-cm^{-1} pyrene band exhibits an enhancement of its saturation compared to the other pyrene bands. This results because of the larger intensity of the 592-cm^{-1} band for pyrene bound to the external site; this environment is similar to that of a moderately polar solvent environment which also shows a large 592-cm^{-1} band intensity. We can simply interpret all of our results in terms of separate spectral contributions from the intercalated and the external site bound pyrenes. The external site bound pyrene selectively contributes to the fluorescence and shows selective ground-state depletion in the high pulse energy flux excitation Raman measurements. The increased saturation for the 592-cm^{-1} band compared to the other pyrene bands derives from the larger 592-cm^{-1} cross sections for the external site bound species than for the intercalated pyrene. The major contribution to the 240-nm absorption band of Figure 1C is the higher concentration of intercalated pyrene. The external site bound component is spectroscopically less perturbed by excitonic interactions than the intercalated pyrene. Thus, the external site bound pyrene shows little change in absorption and Raman excitation profile width or excitation profile maximum. Since we are exciting at the 592-cm^{-1} excitation profile maximum, we will see a maximum 592-cm^{-1} relative intensity. The results of our pump–probe Raman decoupling experiments in Figure 9 support this interpretation. By introducing high-power pump excitation at the absorption peak of the external site bound pyrene, we selectively decoupled the external site bound pyrene with the longer S_1 lifetime.

This selective saturation allows us to selectively observe the spectral signatures of the external site bound pyrene relative to the intercalated pyrene. The Raman difference spectrum between low power and high power selectively shows the Raman bands of the external site bound pyrene. In contrast, the high power flux excited spectrum is enriched in the contribution of the intercalated pyrene. This permits us to saturate out differentially different pyrene constituents in the sample. We can then monitor the relative intensities of the Raman bands and can examine the frequencies to determine environment and intermolecular interactions.

We estimated the Raman cross sections of the intercalated and external site bound pyrene by utilizing a saturation expression which includes two species: a nonsaturating intercalated pyrene and a saturating external site bound pyrene (which constitutes 7% of the pyrenes in the sample). We can estimate the absorption cross section for the intercalated pyrene from the Figure 1 absorption spectrum. The remaining parameters derive from the saturation model fit. The last two columns of Table II list the calculated Raman cross sections of intercalated and external site bound pyrene and demonstrate the large Raman hypochromism which occurs for the intercalated pyrene, especially for the 592-cm^{-1} band. Significant differences are also evident for the estimated cross sections of the external site bound pyrene relative to pyrene in SDS micelles. In the future we will examine the excitation profiles of the saturation to monitor the changes in the external site bound pyrene absorption spectrum that causes the alterations in the relative cross sections of the 592- and 1632-cm^{-1} bands. This will give additional information on interactions between pyrene and the DNA external site environment.

(49) Siemiarczuk, A.; Ware, W. R. *Chem. Phys. Lett.* **1990**, *167*, 263.
(50) Isenberg, I.; Baird, S. L., Jr.; Bersohn, R. *Biopolymers* **1967**, *5*, 477.
(51) Telser, J.; Cruickshank, K. A.; Morrison, L. E.; Letzel, T. L. *J. Am. Chem. Soc.* **1989**, *111*, 6966.
(52) LeBreton, P. R. *Polycyclic Hydrocarbons and Carcinogenesis*; Harvey, R. G., Ed.; American Chemical Society: Washington, DC; pp 209–238. Abramovich, M.; Prakash, A. S.; Harvey, R. G.; Zegar, I. S.; LeBreton, P. R. *Chem.-Biol. Interact.* **1985**, *55*, 39.

Conclusions

Intercalation of pyrene into DNA results in a strong hypochromism of those pyrene electronic absorption bands which overlap the nucleic acid electronic transitions. The resonance Raman cross sections of pyrene excited within these hypochromically affected absorptions are decreased by factors of 10–100-fold. Raman saturation measurements indicate a dramatic increase in the intercalated pyrene nonradiative relaxation rate, which is consistent with the fluorescence quenching observations. We demonstrate using the new technique of optical decoupling Raman spectroscopy (ODRS) that the remaining fluorescence derives from pyrenes not intercalated between bases, but most likely bound at the DNA minor groove. ODRS involves a double pulse sequence, where the pump laser excites the sample at a wavelength selectively absorbed by a particular component, to remove it from its electronic ground state. A probe pulse monitors the Raman spectra of the remaining ground-state species in the sample, in this case intercalated pyrene. The Raman intensities and enhancement patterns of the intercalated pyrene are very different from those of the external site bound pyrene. This new technique of ODRS permits us to selectively monitor pyrene molecules bound at two different sites of DNA and is a new general method for studying complex systems.

Acknowledgment. We thank Richard Bormett and Sunho Song for technical help and acknowledge support for this work from NIH Grant 1RO1GM30741-11.